

First-principles calculations of the thermodynamic and structural properties of strained $\text{In}_x\text{Ga}_{1-x}\text{N}$ and $\text{Al}_x\text{Ga}_{1-x}\text{N}$ alloys

L. K. Teles,^{1,2} J. Furthmüller,¹ L. M. R. Scolfarro,² J. R. Leite,² and F. Bechstedt¹

¹Institut für Festkörpertheorie und Theoretische Optik, Friedrich-Schiller-Universität, 07743 Jena, Germany

²Universidade de São Paulo, Instituto de Física CP66318, 05315-970 São Paulo SP, Brazil

(Received 8 November 1999; revised manuscript received 2 March 2000)

We present first-principles calculations of the thermodynamic and structural properties of cubic $\text{In}_x\text{Ga}_{1-x}\text{N}$ and $\text{Al}_x\text{Ga}_{1-x}\text{N}$ alloys. They are based on the generalized quasichemical approach to disorder and composition effects and a pseudopotential-plane-wave approximation for the total energy. The cluster treatment is generalized to study the influence of biaxial strain. We find a remarkable suppression of phase separation in $\text{In}_x\text{Ga}_{1-x}\text{N}$.

I. INTRODUCTION

During the past few years remarkable progress has been made in the development of optical and electronic devices based on group-III nitrides AlN, GaN, and InN. Important examples are active optoelectronic devices operating in the green, blue and ultraviolet spectral region.¹ Moreover, high-frequency and high-temperature electronic devices as field-effect transistors have been proposed.² A common feature of these device structures is the use of ternary $\text{In}_x\text{Ga}_{1-x}\text{N}$ or $\text{Al}_x\text{Ga}_{1-x}\text{N}$ alloys. Alloying among the group-III nitrides allows in principle to change the band gap from about 1.89 eV in InN to 6.28 eV in AlN with an intermediate value 3.44 eV for GaN (at 300 K).³

For group-III nitride mixed crystals there are strong indications for a miscibility gap.^{4–7} In a closely lattice matched $\text{Al}_x\text{Ga}_{1-x}\text{N}$ system the critical temperature for the occurrence of a miscibility gap was shown to be rather low⁸ and, hence one may expect to have more or less a true solid solution under normal conditions. In $\text{In}_x\text{Ga}_{1-x}\text{N}$ alloys, however, phase separation effects have been observed experimentally in a wide composition range.^{9–11} Recently, such ordering phenomena have been also reported for the $\text{Al}_x\text{Ga}_{1-x}\text{N}$ system: Instead of a random alloy, for an intermediate composition region a tendency for the formation of self-organized superlattice structures has been found.¹²

Under ambient conditions AlN, GaN, and InN crystallize in the hexagonal wurtzite (2H) structure. The ternary alloys grow also in wurtzite structure independent of the deposition technique: molecular beam epitaxy (MBE),⁹ metal-organic chemical vapor phase deposition,¹³ and hydride vapor phase epitaxy (HVPE).¹⁴ Recent epitaxy of thin AlN, GaN, and InN films has been demonstrated to result in the cubic zinc-blende (3C) structure.¹⁵ The remarkable progress in the synthesis of such 3C-GaN films,^{16,17} but also 3C-AlN¹⁸ and 3C-InN^{19,20} layers is related to the plasma-assisted MBE on GaAs(001) or 3C-SiC(001) substrates. Meanwhile, also ternary cubic $\text{Al}_x\text{Ga}_{1-x}\text{N}$ as well as $\text{In}_x\text{Ga}_{1-x}\text{N}$ layers have been deposited.^{18,21,22}

A common feature of the nitride alloy epitaxies is the strain due to lattice mismatch and different thermal expansion coefficients. The lattice mismatch between GaN and

AlN is 2.5% and 4.1% for the hexagonal *a* and *c* lattice constants, respectively. The lattice mismatch increases to 10.7% and 15% (about 10.4% in the cubic case) between InN and GaN. The thermal expansion coefficients vary between 5.6 (3.2) and 4.2 (5.3) $\times 10^{-6}$ K for the *a*-axis (*c*-axis) direction in hexagonal GaN and AlN.³ The large differences in the equilibrium lattice constants and expansion coefficients result in several consequences. First, due to the very different bond lengths, a considerable internal strain arises. It drives the tendency of the ternary nitrides to phase separation. Second, already small contributions of another group-III element into a compound give rise to remarkable changes of the lattice constant. As a consequence, an epitaxial layer of a ternary nitride grown pseudomorphically on a binary system becomes highly strained. Its growth process as well as its properties are influenced. Recent investigations have revealed a compositional pulling effect in $\text{In}_x\text{Ga}_{1-x}\text{N}$ due to the lattice-mismatched growth.^{23,24} The accompanying composition variations in space influence the optical properties.²⁵ The compositional splitting may even result in the existence of InN inclusions in $\text{In}_x\text{Ga}_{1-x}\text{N}$ epilayers grown on sapphire (0001) substrates.²⁶ Strain and composition fluctuations influence all types of properties of the nitride alloys including the miscibility. Theoretical studies of the $\text{In}_x\text{Ga}_{1-x}\text{N}$ alloys performed within the framework of the valence force field (VFF) approximation indicate a shift of the miscibility gap into the area of higher InN concentration²⁷ or lower InN concentration²⁸ in dependence on the details of the simplified calculation. Structurally the first- and second-nearest-neighbor distances are influenced.^{29–31}

In this paper we present a rigorous theoretical study of thermodynamic and structural properties of strained $\text{In}_x\text{Ga}_{1-x}\text{N}$ and $\text{Al}_x\text{Ga}_{1-x}\text{N}$ alloys. The interplay of composition fluctuations, miscibility and strain influence is discussed. Contrary to previous works performed so far, the calculations carried out here taking strain effects into account are based on first-principles methods. The so-called generalization of the quasichemical approximation is adopted to treat disorder and composition effects. We investigate the influence of a biaxial strain on the miscibility of the alloy using a microscopic model. In the work we discuss the length scale

and the limiting situations of the strain influence within a cluster expansion method. In Sec. II we describe the calculational methods, whereas a detailed discussion of the alloy behavior and properties as well as of the strain influence is given in Sec. III. Finally, in Sec. IV a brief summary is given.

II. CALCULATIONAL METHODS

A. Cluster expansion

We consider a pseudobinary nitride alloy $X_x\text{Ga}_{1-x}\text{N}$ ($X = \text{In}, \text{Al}$), which crystallizes nearly in a tetrahedrally coordinated lattice. We assume the cubic zinc-blende structure. However, the results can be immediately transferred to a tetragonal system. Explicitly we study zinc-blende crystals biaxially strained in the direction of a cubic axis. The alloy atoms X and Ga should randomly occupy their fcc sublattice sites while the N atoms occupy the other fcc sublattice. In reality, even in an unstrained alloy the sublattices deviate from the ideal fcc structure,^{28–30,32} and the distribution of the X and Ga atoms over the cation sublattice may be never random.

The Helmholtz free energy F of the system can be divided into two contributions, $F = F_0 + \Delta F$, for each volume V , temperature T , and X molar fraction x . The contribution

$$F_0(x, T) = (1 - x)F_{\text{GaN}}(T) + xF_{\text{XN}}(T) \quad (1)$$

describes the free energy of a macroscopic mixture of the two binary constituents. The free energies F_{GaN} and F_{XN} can be calculated using standard thermodynamic properties of binary compounds. The microscopic intermixing of the different cations is given by the free-energy contribution

$$\Delta F(x, T) = \Delta U(x, T) - T\Delta S(x, T), \quad (2)$$

where ΔU is the mixing internal energy and ΔS denotes the mixing entropy. The difference ΔU can be also identified with the mixing enthalpy of the alloy.

The knowledge of the free energy $F(x, T)$ allows the construction of a T - x phase diagram of the $X_x\text{Ga}_{1-x}\text{N}$ system.³³ Since $\Delta U(x, T) > 0$ at $T = 0$ K holds for typical semiconductor alloys, a critical temperature T_{crit} exists. For temperatures $T > T_{\text{crit}}$ random alloys with any molar fraction x are stable. However, for a temperature $T < T_{\text{crit}}$ a miscibility gap for x within the interval $x_1 < x < x_2$ should occur. The compositions x_1 and x_2 are the points at which the common tangent touches the $F(x, T)$ curve. With the definition of the chemical potential $\mu(x, T) = (\partial/\partial x)F(x, T)$ it therefore holds

$$\mu(x_1, T) = \mu(x_2, T). \quad (3)$$

The two branches $x_1 = x_1(T)$ and $x_2 = x_2(T)$ define the binodal line in the phase diagram. For a given temperature the alloy $X_x\text{Ga}_{1-x}\text{N}$ is thermally stable against decomposition for X molar fractions $x \leq x_1$ and $x \geq x_2$. Inside the interval the mixture of the two alloys $X_{x_1}\text{Ga}_{1-x_1}\text{N}$ and $X_{x_2}\text{Ga}_{1-x_2}\text{N}$ possesses the free energy

$$F_{\text{mix}}(x, T) = \frac{x_2 - x}{x_2 - x_1}F(x_1, T) + \frac{x - x_1}{x_2 - x_1}F(x_2, T), \quad (4)$$

which is lower than that of the alloy with the averaged composition x , i.e., $F_{\text{mix}}(x, T) < F(x, T)$ within $x_1 < x < x_2$. There are two other special molar fractions, x'_1 and x'_2 , defined at the inflection points of $F(x, T)$ and $\Delta F(x, T)$ at each $T < T_{\text{crit}}$, i.e.,

$$\frac{\partial^2}{\partial x^2}F(x, T) = \frac{\partial^2}{\partial x^2}\Delta F(x, T) = 0 \quad (5)$$

at these composition x values.³⁴ The branches $x'_1 = x'_1(T)$ and $x'_2 = x'_2(T)$ define the spinodal curve. In the intervals $x_1 < x < x'_1$ and $x_2 < x < x'_2$ the alloy is metastable against local decomposition. An energy barrier exists. On the other hand, spontaneous decomposition into alloys with the averaged compositions x_1 and x_2 happens within the interval $x'_1 < x < x'_2$.

In order to describe the mixing free energy (2) of a random alloy we follow a cluster expansion approach,^{35,36} the so-called generalized quasichemical approximation (GQCA).³⁷ In this approximation the considered mixed crystal $X_x\text{Ga}_{1-x}\text{N}$ is divided into an ensemble of clusters, each of which is taken to be independent statistically and energetically of the surrounding atomic configuration. In the sense of a random alloy the material is assumed to be spatially homogeneous everywhere on a macroscopic (or at least mesoscopic) length scale. In the cation sublattice we consider N sites on which the $X = \text{In}, \text{Al}$, and Ga atoms assume some configuration. The numbers of X and Ga atoms are

$$N_X = xN,$$

$$N_{\text{Ga}} = (1 - x)N, \quad (6)$$

$$N = N_X + N_{\text{Ga}}.$$

We first compose the system in M clusters of $2n$ -atoms ($N = nM$) each which are treated independently. For a given alloy configuration the clusters can be arranged in $(J+1)$ classes with distinct total energies of the clusters, ε_j with $j = 0, 1, \dots, J$. In each class there are M_j clusters with the same energy ε_j . It holds $M = \sum_j M_j$. Introducing the fraction $x_j = M_j/M$ of clusters of energy ε_j , the last equation can be written as

$$\sum_{j=0}^J x_j = 1. \quad (7)$$

Besides in energy the clusters can also differ with respect to the number n_j of X atoms and the number $(n - n_j)$ of Ga atoms, respectively. These numbers underly a constraint due to the given averaged composition x , i.e., the X molar fraction, as

$$\sum_{j=0}^J n_j x_j = nx. \quad (8)$$

According to the Connolly-Williams method,³⁸ the constraint (8) can be interpreted as a special case of the repre-

sentation of the configurationally averaged and hence composition-dependent (and in general also temperature-dependent) value

$$P(x, T) = \sum_{j=0}^J x_j P_j \quad (9)$$

of a property P of interest for the pseudobinary alloy with mainly compositional disorder. Such a property is different for each cluster, depends on the cluster class index j , and hence gives rise to P_j . In the case of Eq. (8) it holds $P_j = n_j/n$ and $P(x, T) = x$. The definition of the configurational average allows the introduction of fluctuations around the mean values by considering the mean-square (rms) deviations

$$\Delta P(x, T) = \left\{ \sum_{j=0}^J x_j P_j^2 - \left[\sum_{j=0}^J x_j P_j \right]^2 \right\}^{1/2}. \quad (10)$$

The definition (9) has also consequences for the total energy (more strictly the internal energy) of the alloy consisting of $2N$ atoms. For the alloy configured within the set of clusters M_0, M_1, \dots, M_J it holds

$$U(x, T) = \sum_{j=0}^J M_j \varepsilon_j. \quad (11)$$

Divided by the number M of clusters in the alloy, Eq. (11) corresponds to the definition of the averaged energy of a cluster according to Eq. (9) and the definition $x_j = M_j/M$. The representation (11) corresponds formally to the description of a many-particle system, which can be described in a single-particle approximation of independent particles with energies ε_j . Equation (11) corresponds to the second assumption of the GQCA, that the energy of each cluster is independent of its environment. In this approach the total mixing internal energy is then

$$\Delta U(x, T) = \sum_{j=0}^J M_j \varepsilon_j - M[(1-x)\varepsilon_0 + x\varepsilon_J]. \quad (12)$$

B. Statistics

The configurational or mixing entropy can be calculated from the Boltzmann definition $\Delta S(x, T) = k_B \ln W$, where W is the number of ways to configure the alloy with the set M_0, M_1, \dots, M_J of clusters.³⁷ This number W of configurations is given by the total number of ways $N!/(N_X! N_{Ga}!)$, in which N_{Ga} Ga atoms and N_X X atoms can be placed on N sites. First, this number has to be multiplied by the probability $M!/\prod_{j=0}^J M_j!$, i.e., the fraction of ways to arrange the different clusters M_0, M_1, \dots, M_J . Second, with the assumption that the various clusters are independent, one has to multiply by the joint probability of finding the set of clusters M_0, M_1, \dots, M_J in the alloy $\prod_{j=0}^J (x_j^0)^{M_j}$ with

$$x_j^0 = g_j x^{n_j} (1-x)^{4-n_j} \quad (13)$$

the fraction of clusters of type j for a given composition x in a regular solid solution. The degeneracy factor g_j is the number of ways of arranging the alloying cations in a cluster with energy ε_j . Summarizing it holds

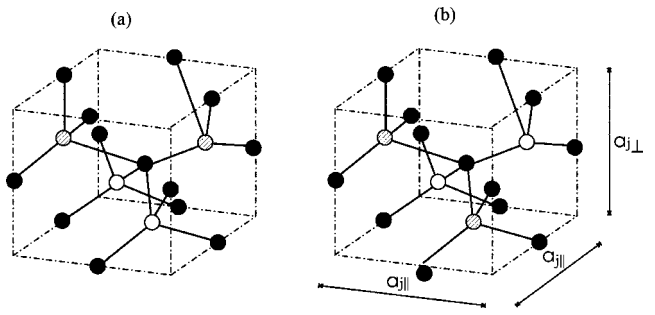


FIG. 1. Schematic representation of 16-bond or 8-atom clusters in a pseudobinary $X_xGa_{1-x}N$ alloy. The figure shows two possible clusters (a) and (b) with $n_j=2$, $X=In, Al$ atoms (shaded circles) and $(4-n_j)=2$ Ga atoms (open circles). The N atoms are represented by filled circles. The presence of a possible biaxial strain parallel to the [001] direction is indicated by the two different lattice constants $a_{j||}$ and $a_{j\perp}$ in (b).

$$W = \frac{N!}{N_X! N_{Ga}!} \frac{M!}{\prod_{j=0}^J M_j!} \prod_{j=0}^J (x_j^0)^{M_j}. \quad (14)$$

In the Stirling limit it follows for the mixing entropy

$$\Delta S(x, T) = -k_B \left\{ N[x \ln x + (1-x) \ln(1-x)] + M \sum_{j=0}^J x_j \ln \left(\frac{x_j}{x_j^0} \right) \right\}. \quad (15)$$

We mention that for $x_j = x_j^0$ the GQCA expression (15) changes over into the mixing entropy of the ideal solution model.³⁴

The cluster fractions x_j are unknown. However, they can be interpreted as variational parameters. Then, by minimizing the free energy (or the mixing free energy) under the constraints (7) and (8), one finds ($\beta = 1/k_B T$)

$$x_j = \frac{\sum_{j=0}^J g_j \eta^j e^{-\beta \varepsilon_j}}{\sum_{j=0}^J g_j \eta^j e^{-\beta \varepsilon_j}}. \quad (16)$$

The unknown parameter η has to be determined from the condition that expression (16) fulfills the constraint (8). In the high-temperature limit $\beta \rightarrow 0$, it holds $\eta = x^{n_j}(1-x)^{4-n_j}$ and the fractions x_j (16) are equal to the probabilities of a random cluster distribution (13). The mixing entropy (15) becomes that of an ideal solid solution.

C. Clusters for strained and unstrained alloys

Within the GQCA the size and the shape of the clusters with the energy ε_j used are important. Four-bond clusters centered at the alloying X and Ga atoms are too small. Such clusters do not yield information about the local correlation of the cations. The smallest clusters that consider local correlation are 16-bond clusters with a central N atom and four alloying atoms bound to the environment by 12 second-neighbor N atoms.³⁴ These clusters are schematically shown in Fig. 1. There is another advantage using such 16-bond or

8-atom clusters, $X_{n_j}Ga_{4-n_j}N_4$ with $n=4$. Their choice means that the counting scheme (14) for the configurational entropy (15) is exact, since no two clusters share the same alloying atoms; in other words, since the cluster surfaces are chemically ordered.

In the absence of external stresses, there are five kinds $j = 0, \dots, 4$ ($J=4$) of clusters distinguished by distinct cluster energies ε_j . These clusters can be labeled according to the numbers n_j and $(4-n_j)$ of different cations, $X_0Ga_4N_4$, $X_1Ga_3N_4$, $X_2Ga_2N_4$, $X_3Ga_1N_4$, and $X_4Ga_0N_4$ with $n_j=j=0,1,2,3,4$ and $n=J=4$. The degeneracy factors are $g_j={4\choose j}=4!/j!(4-j)!$, i.e., $g_0=1$, $g_1=4$, $g_2=6$, $g_3=4$, and $g_4=1$. Each cluster occupies one cube in the crystal. The total number of clusters is $M=N/4$. The cluster energies ε_j can be calculated using a supercell method, where the system consists only of supercells corresponding to one and the same cluster under consideration. The cluster energies $\varepsilon_j=\varepsilon_j(a_j)$ depend on the cubic lattice constant a_j . In our approach the crystals consisting of clusters $X_2Ga_2N_4$ correspond to $(XN)_1(GaN)_1(001)$, (010) or (100) superlattices. Because of their simple tetragonal structure, one has to optimize the total energy at least with respect to two different lattice constants. However, the energies of these superlattices are nearly the same. Moreover, an arithmetic average over the six $X_2Ga_2N_4$ superlattices gives again practically a cubic system. Therefore, since we have to determine an averaged cubic lattice constant for the total alloy system, we neglect the differences in the lattice constants parallel and perpendicular to the superlattice axis and work only with an averaged cluster $j=2$ with an averaged cubic lattice constant a_2 , at least in the strain-free situation.

In the calculation of ε_j we replace a_j by the equilibrium one obtained by minimizing the total energy of a crystal only consisting of clusters of kind j . That means, we assume that each cluster occurring in the alloy takes its equilibrium volume independent of the averaged atomic distances in other regions of the alloy. According to the general definition of the configurational average (9) the composition- and slightly temperature-dependent lattice constant $a=a(x,T)$ of the pseudobinary nitride alloy follows as

$$a = \sum_{j=0}^J x_j a_j \quad (17)$$

with the equilibrium lattice constants a_j of the various cluster kinds. We have also tested the choice of a unique lattice constant for all clusters. The minimization of the corresponding free energy $F(x,T)$ gives an averaged lattice constant that indeed fulfills Vegard's rule. However, this free energy does not give the minimum energy of the system in contrast to the method used by us here. These findings are in agreement with more general predictions.³⁶

The described method has an additional advantage. In principle, in the total energy calculations using a cube only the inside cations are allowed to relax to account for the bond length alternation. Thus, for a given cube the second-nearest neighbor relaxation in the alloyed sublattice is neglected. However, we go beyond this limitation. We relax the second-nearest neighbor distances by assuming different volumes for the various configurations. It has been found for

$GaAs_xSb_{1-x}$ (Ref. 39) that this relaxation releases a lot of the strain energy stored in the tetrahedra and leads to excellent agreement between theoretical and experimental phase diagrams.

There is another advantage of the 16-bond clusters. They allow to model easily the presence of strain in each cluster. We consider a biaxial strain parallel to the cubic [001] direction that deforms the cubes. Consequently, the crystals consisting of a certain cluster kind become tetragonal symmetry. One has to study two lattice constants $a_{j\parallel}$ and $a_{j\perp}$ different from the equilibrium lattice constant a_j in the strain-free case. The resulting strain tensor remains diagonal and possesses the two independent components $\epsilon_{j\parallel}$ and $\epsilon_{j\perp}$.

The presence of the biaxial strain partially lifts the cluster degeneracy in the $j=2$ case. Whereas the total number of clusters distributed over the entire alloy is still $M=N/4$, the number of cluster kinds is increased to $J=5=n+1$. It holds $n_j=j$ for $j=0,1,2$ or $n_j=j-1$ for $j=3,4,5$. The degeneracy factors are $g_0=1$, $g_1=4$, $g_2=2$, $g_3=4$, $g_4=4$, and $g_5=1$. For clusters with one $X=In, Al$ or one Ga atom the cluster energy ε_j with $j=1$ or 4 is independent of the site occupied by this atom. However, in the case of equal numbers $n_2=n_3=2$ of $X=In, Al$ atoms (and, hence, also Ga atoms) different atomic arrangements give rise to different cluster energies $\varepsilon_2 \neq \varepsilon_3$ as indicated in Fig. 1. There are two equivalent planes perpendicular to [001] for the arrangement of two equal cations in Fig. 1(a). If the two atoms in these planes [cf. Fig. 1(b)] are different, four distinct geometries with the same energy are possible.

D. Modeling of macroscopic strain

The modeling of the macroscopic strain behavior is not obvious in the cluster approach. Whereas the treatment of a given strain is well defined on the microscopic length scale of the clusters considered, there are principal difficulties on a macroscopic length scale with characteristic distances larger than the cluster extent, in particular if phase separation may occur in the mixed crystal. Considering epitaxial pseudomorphic growth of a nitride alloy or such an alloy layer with a residual biaxial strain, one automatically discusses the realization of a homogeneous macroscopic strain field characterized by the averaged quantities $\epsilon_{\parallel}(x)$ and $\epsilon_{\perp}(x)$. If phase separation happens, one expects such a strain field defined by the local composition x in each phase. However, different microscopic realizations of such a strain field are imaginable.

For a given alloy with a homogeneous average composition x two extreme limiting situations can be considered for the strain distribution. Assuming a *homogeneous strain distribution* the same in-plane strain occurs in all clusters. The strain tensor component $\epsilon_{j\parallel}=(a_{j\parallel}-a_j)/a_j$ becomes independent of j and takes the same value $\epsilon_{\parallel}(x)$. However, this model cannot completely correctly describe real biaxially strained alloys. In agreement with the assumption that each cluster takes its own equilibrium volume, the strain $\epsilon_{j\parallel}=(a_{\parallel}-a_j)/a_j$ in the clusters should be different. One assumes that, for instance during pseudomorphic growth, the substrate determines (and hence fixes) the in-plane lattice constant a_{\parallel} in each cluster at the same value. Consequently a spatially *inhomogeneous strain relief* occurs. The strain varies locally on a characteristic length of the order of the clus-

ter size. In order to obtain the homogeneous or inhomogeneous strain distributions, we fix the in-plane lattice constant $a_{j\parallel}$ in each cluster and minimize the total energy of the crystal with corresponding cluster supercells with respect to $a_{j\perp}$. The in-plane lattice constant $a_{j\parallel}$ follows either from $\epsilon_{j\parallel} = \epsilon_{\parallel}$ (homogeneous situation) or $a_{j\parallel} = a_{\parallel}$ (inhomogeneous situation).

E. Total energy

The total-energy calculations for each cluster kind are based on the density functional theory (DFT) in the local density approximation (LDA).⁴⁰ Besides the valence electrons also the semicore Ga 3d and In 4d states are explicitly considered. Their interaction with the atomic cores is treated by non-normconserving *ab initio* Vanderbilt pseudopotentials.⁴¹ They allow a substantial potential softening also for first-row elements with the lack of core p electrons as well as for the attraction of shallow d electrons.⁴² As a consequence of the optimization the plane-wave expansion of the single-particle eigenfunctions may be restricted by an energy cutoff of 22.2 Ry for all nitrides and their alloys. The cutoffs have been carefully tested in the case of bulk structures, cleavage and basal-plane surfaces.⁴³ However, to be on the safe side the cutoff is substantially increased since in the ternary alloy case shorter bond lengths as in the binary nitrides occur. The electron-electron interaction is described within the Ceperley-Alder scheme as parametrized by Perdew and Zunger.⁴⁴ The \mathbf{k} -space integrals are approximated by sums over a $5 \times 5 \times 5$ special-point mesh of the Monkhorst-Pack type⁴⁵ within the irreducible part of the Brillouin zone (BZ). Our calculations employ the conjugate-gradient method to minimize the total energy. Explicitly we use the Vienna Ab-initio Simulation Package.⁴⁶

In order to determine the cluster energies $\epsilon_j = \epsilon_j(a_{j\parallel}, a_{j\perp})$ the lattice constants $a_{j\parallel}$ and $a_{j\perp}$ are kept fixed in a first step. All atomic coordinates in the supercell are relaxed until the Hellmann-Feynman forces vanish. In a second step the total energy is minimized with respect to $a_{j\perp}$ using a parabola fit. For each cluster j , the second linearly independent component of the diagonal strain tensor follows from the relation $\epsilon_{j\perp} = (a_{j\perp} - a_j)/a_j$. The diagonal elements of the stress tensor

$$\begin{aligned} \sigma_{j\parallel} &= (c_j^{11} + c_j^{12})\epsilon_{j\parallel} + c_j^{12}\epsilon_{j\perp}, \\ \sigma_{j\perp} &= 2c_j^{12}\epsilon_{j\parallel} + c_j^{11}\epsilon_{j\perp} \end{aligned} \quad (18)$$

with the elastic stiffness constants $c_j^{\alpha\beta}$ give with the boundary condition, $\sigma_{j\perp} = 0$, the relation

$$\epsilon_{j\perp} = -2(c_j^{12}/c_j^{11})\epsilon_{j\parallel}. \quad (19)$$

The comparison of the $a_{j\perp}$ -lattice constant versus the $a_{j\parallel}$ -lattice constant with Eq. (19) allows the determination of the ratio c_j^{12}/c_j^{11} for each cluster. A measure of the averaged elastic properties, the bulk modulus B_j , follows from the volume dependence of the total energy described by Murnaghan equation of state.⁴⁷ The configurationally averaged quantities, c_{12}/c_{11} and B , are computed by means of Eq. (9).

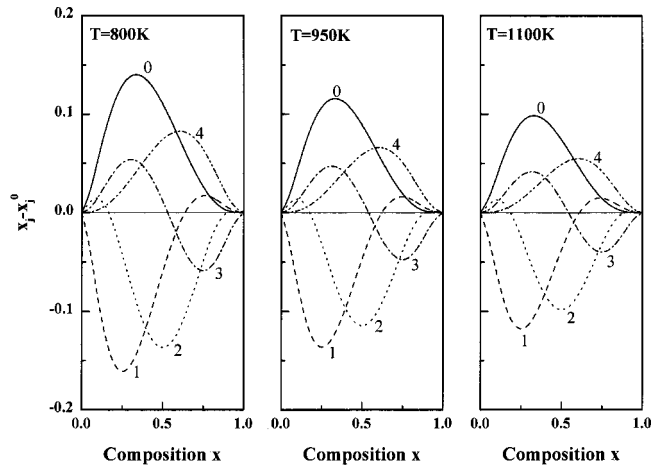


FIG. 2. Excess cluster populations $(x_j - x_j^0)$ for the five clusters $j=0, \dots, 4$ considered for unstrained $\text{In}_x\text{Ga}_{1-x}\text{N}$.

III. RESULTS AND DISCUSSION

A. Equilibrium and fluctuations

We first investigate the randomness of the mixed nitride crystals for the example of unstrained $\text{In}_x\text{Ga}_{1-x}\text{N}$ alloy. The complete randomness is defined by the regular solution model, for which the quantities x_j^0 in Eq. (13) give the *a priori* fractions of clusters of the j th type. Thus, the deviations $(x_j - x_j^0)$ of the randomness are given by the temperature-dependent actual fractions x_j in Eq. (16). These excess probabilities to find clusters of j th kind, $x_j - x_j^0$, are plotted in Fig. 2 for characteristic growth temperatures $T = 800, 950$, and 1100 K. Note that the shapes of the curves at the three temperatures are similar, but the amplitudes of the deviations from the complete random populations are larger for the lower temperatures. The symmetry known for the random probabilities x_j^0 is destroyed. The true cluster fractions x_0 and x_4 as well as x_1 and x_3 are different. This is a consequence of the different cluster energies ϵ_j . In contrast to the $\text{Al}_x\text{Ga}_{1-x}\text{N}$ system the deviations from the random population are substantial in $\text{In}_x\text{Ga}_{1-x}\text{N}$ reflecting the stronger tendency towards clustering. Independent of temperature and composition excess is found for $j=0$ and $j=4$. This is in agreement with the lattice-matched $\text{Al}_j\text{Ga}_{4-j}\text{As}_4$ clusters but in disagreement with other lattice-mismatched III-V compounds.³⁶

The cluster fractions x_j immediately give the mean-square deviation Δx of the composition x according to expression (10). The corresponding results are represented in Fig. 3. They basically show the same dependence as the high-temperature result $\Delta x = \sqrt{x(1-x)/2}$. However, for lower temperatures the composition fluctuations slightly increase and the mirror symmetry with respect to $x=0.5$ is destroyed. The maximum fluctuations occur for molar fractions $x < 0.5$. The two tendencies are again stronger for $\text{In}_x\text{Ga}_{1-x}\text{N}$. In the case of $\text{Al}_x\text{Ga}_{1-x}\text{N}$ the random limit is rather independent of temperature. It should be noted that the large fluctuations obtained are occurring in the length scale of the clusters used.

The cluster energies ϵ_j also define the mixing internal energy (or the mixing enthalpy) according to expression (12). Results for $\Delta U(x, T)$ are plotted in Fig. 4 for $\text{In}_x\text{Ga}_{1-x}\text{N}$. The deviations of ϵ_j from a linear behavior with

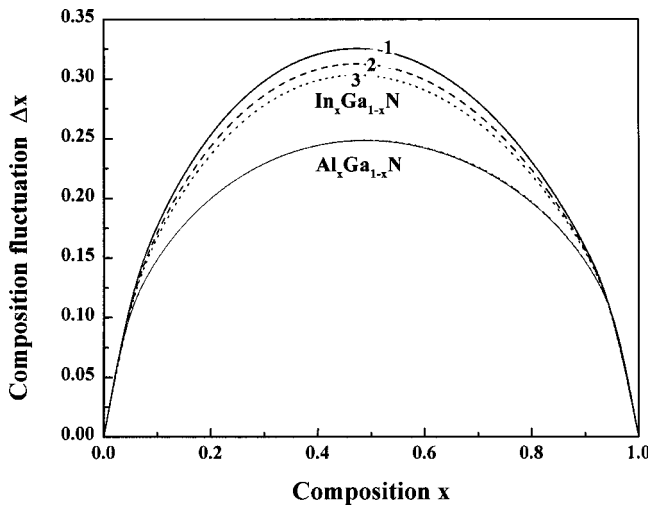


FIG. 3. Mean-square deviations Δx of the averaged composition x in $\text{In}_x\text{Ga}_{1-x}\text{N}$ and $\text{Al}_x\text{Ga}_{1-x}\text{N}$ alloys. Three different temperatures $T=800$ (1), 950 (2), and 1100 (3) K are considered.

the cluster kind j have an important consequence, the mixing enthalpy becomes asymmetric. It cannot anymore be described by an expression such as $\Delta U = \Omega x(1-x)$, as in the case of the ideal solution model.³⁴ Rather a composition-dependent quantity Ω has to be considered. Its maximum value (per cation-anion pair) determines the critical temperature in the mixed crystal by $k_B T_{\text{crit}} = \Omega_{\text{max}}/2$. Hence, the composition dependence of Ω influences the miscibility gap.²⁸ The mixing enthalpy of $\text{Al}_x\text{Ga}_{1-x}\text{N}$ is not plotted in Fig. 4. It is practically zero for all temperatures. Consequently the critical temperature approaches to zero within the GQCA. Within a treatment as a regular solution ($x_j = x_j^0$) we estimate a value $T_{\text{crit}} = 87$ K.

The volume dependence of the cluster energies ε_j gives the bulk moduli B_j (cf. Sec. II E). The corresponding configurationally averaged values as obtained through expression (9) of the isothermal bulk modulus versus composition

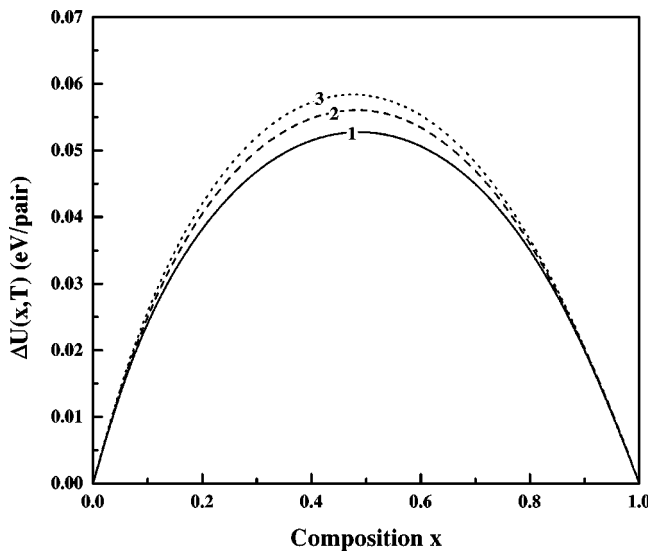


FIG. 4. Mixing enthalpy $\Delta U(x,T)$ for $\text{In}_x\text{Ga}_{1-x}\text{N}$ per cation-anion pair. Three different temperatures $T=800$ (1), 950 (2), and 1100 (3) K are considered.

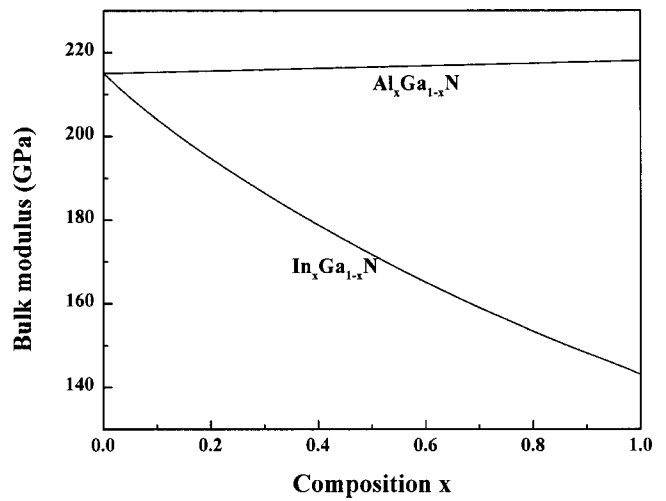


FIG. 5. Bulk modulus B versus composition. The temperature is fixed at $T=950$ K.

are plotted in Fig. 5. Because of the extremely small temperature variation of B , only one temperature $T=950$ K is considered. The composition dependence in the case of $\text{Al}_x\text{Ga}_{1-x}\text{N}$ practically vanishes due to the nearly identical bulk modulus values of the underlying binary nitrides. A bowing occurs for $\text{In}_x\text{Ga}_{1-x}\text{N}$. It nearly holds $B(x) = (1-x)B(\text{GaN}) + xB(\text{InN}) - B_{\text{bow}}x(1-x)$ with $B_{\text{bow}} = 29$ GPa. The values for the binary nitrides are about 10 GPa somewhat larger than values obtained from other calculations.^{5,48-50} Altogether, the weak variation of the bulk modulus with composition can be interpreted as an indication for a reliable approach to the mixed crystals.

Figure 6 depicts the mixing free energy resulting for $\text{In}_x\text{Ga}_{1-x}\text{N}$. The shapes of the curves versus the In molar fraction are asymmetric. Below the critical temperature $T_{\text{crit}} = 1295$ K the excess free energy shows a common tangent at two different x values indicating the tendency for phase decomposition, i.e., the occurrence of a miscibility gap. According to expressions (3), (4) and (5) the knowledge of the free energies allows the construction of a phase diagram. Because of the low value T_{crit} this is somewhat unrealistic for $\text{Al}_x\text{Ga}_{1-x}\text{N}$. The $T-x$ phase diagram resulting for $\text{In}_x\text{Ga}_{1-x}\text{N}$ is represented in Fig. 7. More in detail Fig. 7

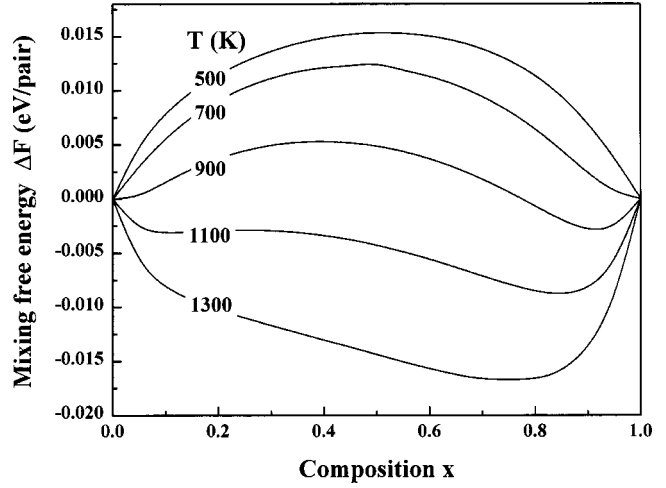


FIG. 6. Mixing free energy $\Delta F(x,T)$ of $\text{In}_x\text{Ga}_{1-x}\text{N}$ alloys versus composition.

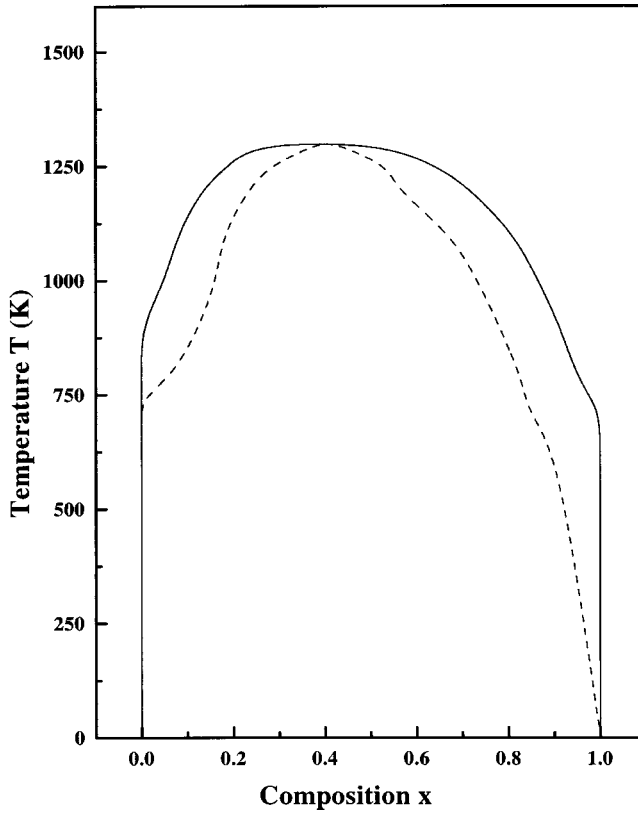


FIG. 7. T - x phase diagram of $\text{In}_x\text{Ga}_{1-x}\text{N}$ ternary alloy system. Solid line: binodal curve; dashed line: spinodal curve.

shows the spinodal and binodal curves calculated within the GQCA and the *ab initio* total energy method. The spinodal curve in the phase diagram marks the equilibrium solubility limit, i.e., the miscibility gap. For temperatures and compositions above this curve a homogeneous random alloy is predicted. In the temperature-composition area below the binodal curve spontaneous decomposition occurs into alloys with fixed compositions defined by the spinodal curve at the considered temperature. The phase separation, which should occur at growth temperatures in $\text{In}_x\text{Ga}_{1-x}\text{N}$, is driven by the internal strain due to the mixing of the two lattice-mismatched components InN and GaN . For $x \leq 0.5$ ($x \gtrsim 0.5$) indium (gallium) atoms are excluded from the $\text{In}_x\text{Ga}_{1-x}\text{N}$ lattice to form alloys of different compositions, hence, locally the strain is reduced, with a consequent reduction of the strain energy of the system.

More in detail, for a typical growth temperature of $T = 1000$ K the solubility limit of InN (GaN) in GaN (InN) is less than 5% (10%). However, the phase diagram also indicates that in a wider range between spinodal and binodal curves the random alloy may exist as a metastable phase. The decomposition tendency is much larger for an In content of 16 until 75%. Such a picture is in agreement with experimental findings.^{9,13,51–53} The phase diagram depicted in Fig. 7 is also similar to that obtained by other authors.^{4,5,28} The main difference to the results of the other DFT-LDA calculations⁵ is due to regular-solution model used in Ref. 5 and the calculation of the mixing enthalpy by using only one alloy configuration. The agreement with Ho and Stringfellow⁴ as well as Saito and Arakawa²⁸ is surprising because these authors perform the calculations within a VFF

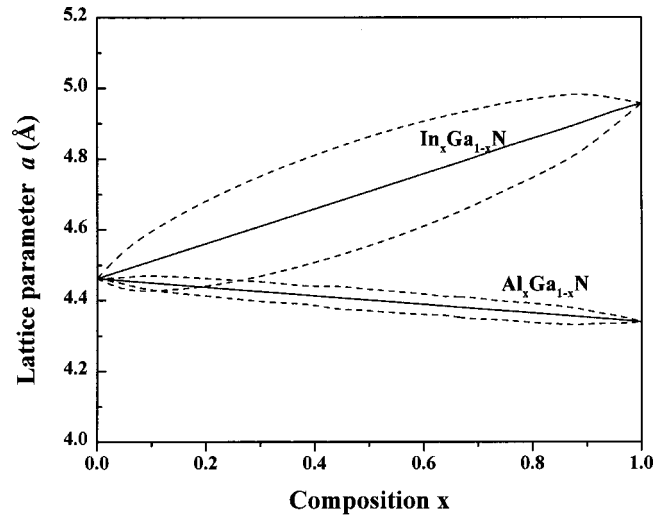


FIG. 8. Configurationally averaged lattice parameter a versus composition x for $\text{In}_x\text{Ga}_{1-x}\text{N}$ and $\text{Al}_x\text{Ga}_{1-x}\text{N}$. The temperature $T = 950$ K is assumed. The range of the fluctuations in the lattice constant is indicated by dashed lines.

method and the regular-solution limit. However, our phase diagram in Fig. 7 is much more asymmetric than the other ones. In particular, we obtain a larger range of miscibility for higher In molar fractions x . Moreover, the phase boundaries are much steeper for $x \rightarrow 0$ and $x \rightarrow 1$ than for ideal alloys. These observations are consequences of the more asymmetric excess internal energy shown in Fig. 4 and the use of the GQCA for the alloy statistics.

B. Structural parameters

Discussing the structural properties of the ternary nitride alloys we focus our attention to the configurationally averaged quantities, lattice constant a , bond lengths d_{X-N} and $d_{\text{Ga-N}}$, as well as second-nearest-neighbor (2NN) distances d_{X-X} , $d_{X-\text{Ga}}$ and $d_{\text{Ga-Ga}}$. The results are presented in Figs. 8, 9, and 10. In general, the deviations of the bond lengths and

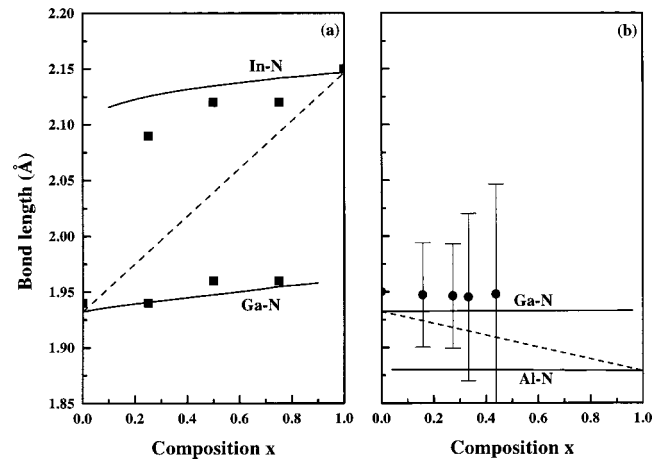


FIG. 9. Averaged bond lengths (solid lines) in $\text{In}_x\text{Ga}_{1-x}\text{N}$ (a) and $\text{Al}_x\text{Ga}_{1-x}\text{N}$ (b) versus composition. The temperature $T = 950$ K is assumed. The dashed line corresponds to the fictitious common bond length according to Vegard's rule. The filled squares (Ref. 32) and circles (Ref. 54) describe measured values. Vertical lines correspond to experimental error bars.

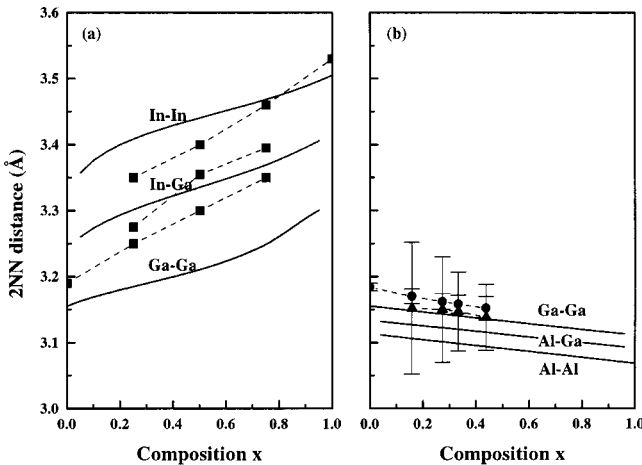


FIG. 10. Averaged second-nearest-neighbor distances (solid lines) in $In_xGa_{1-x}N$ (a) and $Al_xGa_{1-x}N$ (b) versus composition. The temperature $T=950$ K is assumed. The filled squares³² and circles/triangles (Ref. 54) describe measured values. Vertical lines correspond to experimental error bars. Dashed lines linking the measured values are to guide the eyes.

2NN distances are more important for $In_xGa_{1-x}N$. The changes are much smaller in the $Al_xGa_{1-x}N$ case due to the smaller lattice mismatch between AlN and GaN. The second-nearest neighbor distances d_{N-N} are not given in the figures. Due to the limited size of the considered clusters the change in this length in dependence on the In or Ga atom in between the two nitrogen ones³⁰ cannot be described. The configurationally averaged lattice constants a in Fig. 8 clearly fulfill Vegard's law for both the ternary alloys $In_xGa_{1-x}N$ or $Al_xGa_{1-x}N$. Thereby the influence of the temperature variation is negligible. The curves for other temperatures fall together with the line drawn in Fig. 8. Figure 8 also indicates the influence of the fluctuations Δa of the lattice constant a in dependence on the averaged composition x . Whereas for $Al_xGa_{1-x}N$ these deviations Δa are small compared to the averaged lattice constant a itself, they are nonnegligible in the $In_xGa_{1-x}N$ alloy. For an intermediate composition of $x=0.5$ it holds $\Delta a=0.15$ Å. That means, the mean-square deviation of the lattice constant amounts about 3%. This happens already for a random alloy without any decomposition.

In contrast to the lattice constant the definition of the configurational average (17) has to be generalized for the first- and second-nearest neighbor distances d_{X-Y} , because different types of atomic pairs $X-Y$ exist in one cluster. Rather, it holds

$$d_{X-Y} = \frac{\sum_{j=0}^J x_j n_{X-Y}^j d_{X-Y}^j}{\sum_{j=0}^J x_j n_{X-Y}^j}, \quad (20)$$

where n_{X-Y}^j is the relative number of $X-Y$ distances ($X-N$ bond length, $X-Y$ cation-cation 2NN distances) in the cluster. There are constraints $n_{X-N}^j + n_{Ga-N}^j = 1$ and $n_{X-X}^j + n_{X-Ga}^j + n_{Ga-Ga}^j = 1$ ($X=In$ or Al) for each cluster type j . The characteristic distances d_{X-Y}^j are taken for each cluster from the results of the total-energy optimization. In agreement with

experiment^{32,54} two different bond lengths d_{X-N} ($X=In,Al$) and d_{Ga-N} occur in Fig. 9. Apart from the small overbinding effect due to the used DFT-LDA, there is not only a quantitative agreement with the recent experimental results obtained by means of an extended x-ray absorption fine structure (EXAFS) technique for MBE $In_xGa_{1-x}N$ layers³² but also for $Al_xGa_{1-x}N$ alloys.⁵⁴ The same reasonable agreement can be stated with recent VFF calculations using extremely large supercells.^{28,30} This holds in particular taking into consideration the fluctuations of the bond lengths calculated in accordance with the findings for the lattice constants in Fig. 8. Figure 9 makes obvious that Vegard's rule fails for the bond lengths of both $In_xGa_{1-x}N$ and $Al_xGa_{1-x}N$ as in other III-V ternary alloys (cf. Refs. 36 and 37 and references therein).

The 2NN cation distances d_{X-Y} ($X,Y=Al,Ga,In$) are plotted in Fig. 10 versus composition. These distances also do not follow Vegard's rule. Rather, in $In_xGa_{1-x}N$ ternary alloys four distinct values are observed in Fig. 10(a). The magnitude of d_{X-Y} follows the covalent radii of the contributing atoms. Hence, the sequence of decreasing distances In-In, In-Ga and Ga-Ga occurs. Taking into account the overbinding tendency in DFT-LDA, again qualitative and quantitative agreement with experimental³² and other theoretical^{28,30} predictions can be stated, in particular if the uncertainties due to the length fluctuations and the method of determining the lengths are taken into consideration. Qualitatively the same behavior is observed for $Al_xGa_{1-x}N$ [cf. Fig. 10(b)]. However, the variations are much smaller due to the smaller lattice mismatch between AlN and GaN than InN and GaN. Also the agreement with other calculations³⁰ and measured values^{32,54} is reasonable.

C. Influence of biaxial strain

Again we focus our attention to the ternary $In_xGa_{1-x}N$ alloy system. We expect much stronger changes than in the $Al_xGa_{1-x}N$ case. Due to the minor lattice mismatch between AlN and GaN, the strain-induced changes of the properties of $Al_xGa_{1-x}N$ should be similar to those already known for the binary crystals AlN and GaN. First of all, we show in Fig. 11 the influence of compressive strain on the excess free energy for different temperatures. In the calculation we have assumed that the random alloy is homogeneously strained, i.e., all clusters of different kind j are strained by the same in-plane strain $\epsilon_{||}=-0.01$ or -0.05 . Figure 11 shows that the excess free energy is decreased by the elastic energy due to the build-up strain. At least, there is a tendency towards more negative excess free energies. Consequently the miscibility gap should be decreased. In the corresponding T - x phase diagram (Fig. 12) such a trend is indeed observed. For a small biaxial strain of -1% the critical temperature is practically not changed, comparing with that of the unstrained alloy (Fig. 7). The phase diagram becomes only slightly more asymmetric. The reason is the extremely small elastic energy. However, drastic changes occur for larger biaxial strains, since the strain energy is proportional to the square of the in-plane strain $\epsilon_{||}$. In the case of -5% strain the critical temperature is reduced by about 120 K. Simultaneously the miscibility gap as well as the region of spontaneous decomposition is reduced, in particular for larger In

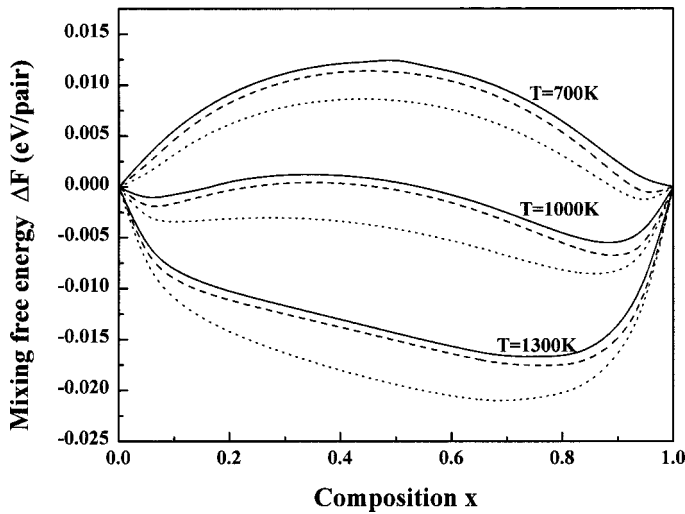


FIG. 11. Mixing free energy of homogeneously strained $\text{In}_x\text{Ga}_{1-x}\text{N}$ alloys versus composition for three different temperatures $T=700$, 1000 , and 1300 K. The biaxial strain is varied $\epsilon_{||}=0.00$ (solid line), -0.01 (dashed line), and -0.05 (dotted line).

molar fractions. One can indeed speak about a tendency for suppression of the phase separation in $\text{In}_x\text{Ga}_{1-x}\text{N}$ due to elastic strain.

There are indications that the assumption of an equal strain in all microclusters of the alloy is not suitable. For instance, we observe a nonlinear behavior of the ratio c_{12}/c_{11} of the elastic stiffness constants versus composition considering both a compressive and a tensile strain of 1%. Only the arithmetic average of the two curves gives an al-

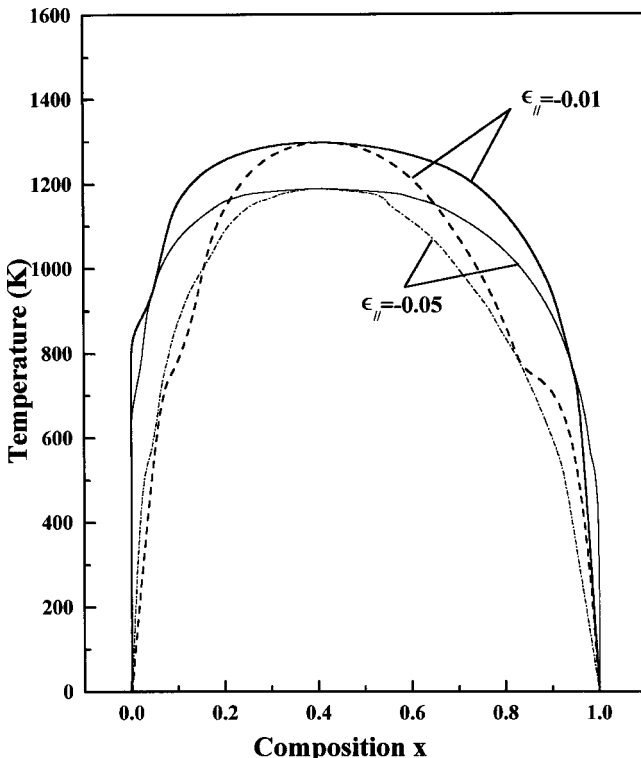


FIG. 12. T - x phase diagram for homogeneously strained $\text{In}_x\text{Ga}_{1-x}\text{N}$. Binodal curves: thick and thin solid lines; spinodal curves: dashed and dot-dashed lines.

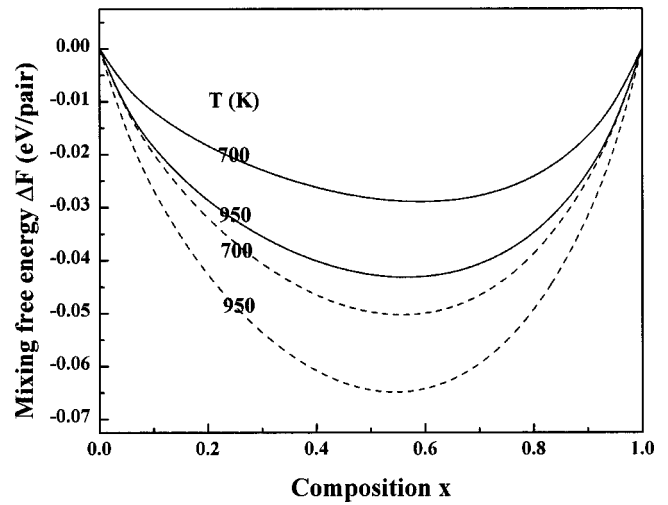


FIG. 13. Mixing free energy of inhomogeneously strained $\text{In}_x\text{Ga}_{1-x}\text{N}$ alloys versus composition for two different temperatures $T=700$ and 950 K. The biaxial strain is defined by $a_{||}=a_{\text{GaN}}$ (solid line) or $a_{||}=a_{\text{InN}}$ (dashed line).

most linear variation of the ratio c_{12}/c_{11} with x between the values known for GaN and InN. Hence, one has also to consider the situation of an inhomogeneous strain distribution in the alloy on a microscopic length scale. In agreement with one of the basic assumptions of the alloy description, that each cluster takes its own volume, we assume a pseudomorphically strained alloy. That means, each cluster j is strained according to the buildup lattice constant $a_{||j}$. The in-plane strain in each cluster is therefore given by $\epsilon_{jj}=(a_{||j}-a_j)/a_j$. In the following we consider two extreme different inhomogeneous strain situations, the pseudomorphic growth of the ternary $\text{In}_x\text{Ga}_{1-x}\text{N}$ alloy on a binary nitride substrate, GaN with $a_{||}=a_{\text{GaN}}$ or InN with $a_{||}=a_{\text{InN}}$.

The resulting thermodynamic potential is represented in Fig. 13. The assumed inhomogeneous strain distribution drastically influences the mixing free energy of the system by changing mainly the mixing enthalpy. Due to elastic energy of each cluster $\sim \epsilon_{jj}^2$ the internal energy of mixing is remarkably reduced, even changing sign, in comparison with the strain-free situation shown in Fig. 6. The free energy exhibits only one minimum at an intermediate molar fraction x . Consequently, the critical temperature T_{crit} of an inhomogeneously strained $\text{In}_x\text{Ga}_{1-x}\text{N}$ alloy approaches values small compared to the growth temperatures or even vanishes. Consequently the ideal random alloy system is stabilized in the entire composition range independent of temperature. One observes not only a suppression of the tendency for phase separation in the pseudomorphically grown alloy layers, but no phase separation for sufficiently large biaxial strain as considered in Fig. 13. This result explains why, for example in $\text{In}_x\text{Ga}_{1-x}\text{N}$ epilayers with In content up to $x=0.3$ and grown at temperatures of 1150–1200 K no evidence for phase separation has been observed.^{9,13}

Since the in-plane lattice constant $a_{||}$ is fixed for each cluster, it also represents the averaged in-plane constant for the entire alloy system. On the other hand, we have determined the lattice constants $a_{j\perp}$ by a total-energy minimization for each cluster. Hence, the averaged lattice constant a_{\perp} of the alloy system can be determined using expression (9).

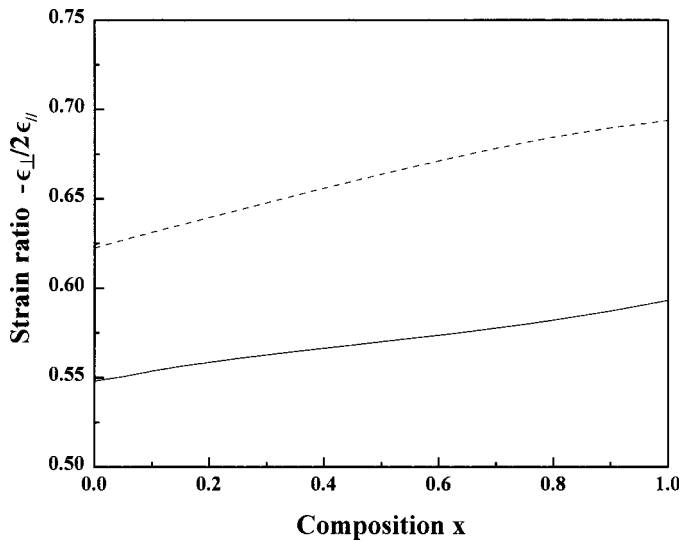


FIG. 14. Macroscopic strain ratio $-\epsilon_{\perp}/2\epsilon_{\parallel}$ versus composition. Solid line: $\text{In}_x\text{Ga}_{1-x}\text{N}$ grown on GaN; dashed line: $\text{In}_x\text{Ga}_{1-x}\text{N}$ grown on InN.

The comparison of the lattice constants a_{\parallel} and a_{\perp} of the strained ternary nitride with the lattice constant $a=a(x)$ of the unstrained alloy yields the macroscopic (in the sense of the configurational average) strain by $\epsilon_{\parallel}=(a_{\parallel}-a)/a$ and $\epsilon_{\perp}=(a_{\perp}-a)/a$. Assuming that Hooke's law is still valid (what is perhaps not true for about 10% strain in certain clusters), the ratio $-\epsilon_{\perp}/2\epsilon_{\parallel}$ defines the ratio c_{12}/c_{11} of the averaged elastic coefficients according to Eq. (19). This ratio is plotted in Fig. 14 versus composition. Indeed in the limit of vanishing strain, i.e., $\text{In}_x\text{Ga}_{1-x}\text{N}$ with $x \rightarrow 0$ grown on GaN and $\text{In}_x\text{Ga}_{1-x}\text{N}$ with $x \rightarrow 1$ grown on InN, the ratios $c_{12}/c_{11}=0.54$ and 0.69 observed for the respective binary nitrides are recovered. These ratios slightly increase (decrease) with rising (decreasing) In molar fraction x for growth on GaN (InN). The weak variation of the ratio $-\epsilon_{\perp}/2\epsilon_{\parallel}$ with composition in Fig. 14 should be interpreted that both important assumptions are reliable, the validity of (i) the 16-bond cluster approach and (ii) the inhomogeneous strain distribution on a microscopic scale. Two reasons can be mentioned. The 8-atom clusters already allow the modelling of the strain on a microscopic scale. The contribution of a microcluster j , for which the assumption of a pseudomorphic strained lattice is perhaps unrealistic, contributes to the random alloy only with a small probability x_j .

IV. SUMMARY

In conclusion, we have presented a combination of different methods to study unstrained and strained ternary

$\text{In}_x\text{Ga}_{1-x}\text{N}$ and $\text{Al}_x\text{Ga}_{1-x}\text{N}$ alloys. We have combined the cluster expansion method with the generalized quasichemical approach and *ab initio* DFT-LDA calculations. Cubes or deformed cubes with eight atoms have been used as basic clusters. They have the advantage of a chemically ordered surface given by the nitrogen second neighbors of a central nitrogen atom. The cluster statistics has been described within the generalized quasichemical method that introduced a temperature dependence of the cluster fractions. The total energy of each cluster has been calculated within a pseudopotential-plane-wave code at the equilibrium lattice constants of each cluster. The configurationally averaged quantities then follow by a summation over the quantity being characteristic for each cluster and weighted by the fractions of clusters. Biaxial strain has been taken into account by fixing the in-plane lattice constant. We considered two different situations, homogeneously strained alloys and inhomogeneously strained alloys, where the strain in each cluster is either equal or different.

Whereas the immiscibility does not play a role for the $\text{Al}_x\text{Ga}_{1-x}\text{N}$ system, we observe a broad miscibility gap for growth temperatures around 1000 K for unstrained $\text{In}_x\text{Ga}_{1-x}\text{N}$ alloys. The critical temperature is about 1295 K. However, there is also a wide range of compositions where a random $\text{In}_x\text{Ga}_{1-x}\text{N}$ alloy may exist as a metastable phase. The resulting structural properties, in particular the composition dependence of the lattice constant, the bond lengths and the second-nearest neighbor distances are in agreement with results of other calculations or measurements. We predict remarkable fluctuations of the structural parameters for intermediate In molar fractions.

A biaxial strain is extremely important for the miscibility behavior of the alloys. In the case of cubic $\text{In}_x\text{Ga}_{1-x}\text{N}$ the strain effects on the immiscibility suppression can be dramatic. This effect is more pronounced for more In-rich samples. In general, the region of spontaneous decomposition is reduced. By considering an inhomogeneous strain distribution over the clusters contributing to the ternary alloy, it is shown that a regular behavior of the structural and elastic properties are obtained. In this limit the miscibility gap and the critical temperature are remarkably reduced. At in-plane lattice constants of the underlying binary compounds the phase separation is even completely suppressed.

ACKNOWLEDGMENTS

We thank A. Zunger for helpful discussions. This work was supported by the Deutsche Forschungsgemeinschaft (Grant No. Be 1346/8-4) and FAPESP, Brazilian funding agency. A part of the numerical calculations has been performed at the supercomputer center NIC Jülich.

¹S. Nakamura and G. Fasol, *The Blue Laser Diode* (Springer, Berlin, 1997).

²M.A. Khan, J.N. Kuznia, D.T. Olson, W.J. Schaff, J.W. Burm, and M. Shur, *Appl. Phys. Lett.* **65**, 1121 (1994).

³*Data in Science and Technology: Semiconductors*, edited by O. Madelung (Springer-Verlag, Berlin, 1991).

⁴I. Ho and G.B. Stringfellow, *Appl. Phys. Lett.* **69**, 2701 (1996); *J. Cryst. Growth* **178**, 1 (1997).

⁵M. van Schilfgaarde, A. Sher, and A.-B. Chen, *J. Cryst. Growth* **178**, 8 (1997).

⁶T. Matsuoka, *Appl. Phys. Lett.* **71**, 105 (1997).

⁷V.A. Elyukhin and S.A. Nikishin, *Semicond. Sci. Technol.* **11**,

- 917 (1996).
- ⁸E.A. Albanesi, W.R.L. Lambrecht, and B. Segall, Phys. Rev. B **48**, 17 841 (1993).
- ⁹R. Singh, D. Doppalapudi, T.D. Moustakas, and L.T. Romano, Appl. Phys. Lett. **70**, 1089 (1997).
- ¹⁰C. Kisielowski, Z. Liliental-Weber, and S. Nakamura, Jpn. J. Appl. Phys. **36**, 6932 (1997).
- ¹¹M.D. McCluskey, L.T. Romano, B.S. Krusor, D.P. Bour, N.M. Johnson, and S. Brennan, Appl. Phys. Lett. **72**, 1730 (1998).
- ¹²B. Neubauer, A. Rosenauer, D. Gerthsen, O. Ambacher, M. Stutzmann, M. Albrecht, and H.P. Strunk, Mater. Sci. Eng., B **59**, 182 (1999); B. Neubauer, A. Rosenauer, D. Gerthsen, O. Ambacher, and M. Stutzmann, Appl. Phys. Lett. **73**, 930 (1998).
- ¹³N.A. El-Masry, E.L. Piner, S.X. Liu, and S.M. Bedair, Appl. Phys. Lett. **72**, 40 (1998).
- ¹⁴Y. Sato and S. Sato, Jpn. J. Appl. Phys., Part 1 **36**, 4295 (1997).
- ¹⁵M.J. Paisley, Z. Sitar, J.B. Posthill, and R.F. Davis, J. Vac. Sci. Technol. A **7**, 701 (1989).
- ¹⁶O. Brandt, H. Yang, B. Jenichen, Y. Suzuki, L. Däweritz, and K. H. Ploog, Phys. Rev. B **52**, R2253 (1995).
- ¹⁷D. Schikora, M. Hankeln, D.J. As, K. Lischka, T. Litz, A. Waag, T. Buhrow, and F. Henneberger, Phys. Rev. B **54**, R8381 (1996).
- ¹⁸H. Okumura, H. Hamaguchi, T. Koizumi, K. Balakrishnan, Y. Ishida, M. Arita, S. Chichibu, H. Nakanishi, T. Nagatomo, and S. Yoshida, J. Cryst. Growth **189/190**, 390 (1998).
- ¹⁹A.P. Lima, A. Tabata, J.R. Leite, S. Kaiser, D. Schikora, B. Schöttker, T. Frey, D.J. As, and K. Lischka, J. Cryst. Growth **201-202**, 396 (1999).
- ²⁰A. Tabata, A.P. Lima, L.K. Teles, L.M.R. Scolfaro, J.R. Leite, V. Lemos, B. Schöttker, T. Frey, D. Schikora, and K. Lischka, Appl. Phys. Lett. **74**, 362 (1999).
- ²¹H. Harima, T. Inoue, S. Nakashima, H. Okumura, Y. Ishida, S. Yoshida, T. Koizumi, H. Grille, and F. Bechstedt, Appl. Phys. Lett. **74**, 191 (1999).
- ²²A. Tabata, J.R. Leite, A.P. Lima, E. Silveira, V. Lemos, T. Frey, D.J. As, D. Schikora, and K. Lischka, Appl. Phys. Lett. **75**, 1095 (1999).
- ²³S. Chichibu, T. Azuhata, T. Sota, and S. Nakamura, in *III-V Nitrides*, edited by F.A. Ponce, T. D. Moustakas, I. Akasaki, and B. A. Monemar, MRS Symposia Proceedings Vol. 449 (Materials Research Society, Pittsburgh, 1997), p. 653.
- ²⁴K. Hiramatsu, Y. Kawaguchi, M. Shimizu, N. Sawaki, T. Zhelleva, R.F. Davis, H. Tsuda, W. Taki, N. Kuwano, and K. Oki, MRS Internet J. Nitride Semicond. Res. **2**, 6 (1997).
- ²⁵N. Wieser, O. Ambacher, H.-P. Felsl, L. Görgens, and M. Stutzmann, Appl. Phys. Lett. **74**, 3981 (1999).
- ²⁶A. Wakahara, T. Tokuda, X.-Z. Dang, S. Noda, and A. Sasaki, Appl. Phys. Lett. **71**, 906 (1997).
- ²⁷S. Yu. Karpov, MRS Internet J. Nitride Semicond. Res. **3**, 16 (1998).
- ²⁸T. Saito and Y. Arakawa, Phys. Rev. B **60**, 1701 (1999).
- ²⁹L. Bellaiche, S.-H. Wei, and A. Zunger, Phys. Rev. B **56**, 13 872 (1997).
- ³⁰T. Mattila and A. Zunger, J. Appl. Phys. **85**, 160 (1999).
- ³¹K. Kim, S. Limpijumnong, W.R.L. Lambrecht, and B. Segall, in *III-V Nitrides* (Ref. 23), p. 929.
- ³²N.J. Jeffs, A.V. Blant, T.S. Cheng, C.T. Foxon, C. Bailey, P.G. Harrison, J.F.W. Mosselmans, and A.J. Dent, in *Wide-Bandgap Semiconductors for High Power, High Frequency and High Temperature*, edited by S. Den Baars, M.S. Shur, J. Palmour, and M. Spencer, MRS Symposia Proceedings Vol. 512 (Materials Research Society, Pittsburgh, 1998), p. 519.
- ³³Ch. Kittel and H. Kroemer, *Thermal Physics* (Freeman, San Francisco, 1980).
- ³⁴A.-B. Chen and A. Sher, *Semiconductor Alloys* (Plenum, New York, 1995).
- ³⁵J.M. Sanchez, F. Ducastelle, and D. Gratias, Physica A **128**, 334 (1984).
- ³⁶A. Zunger, in *Statistics and Dynamics of Alloy Phase Transformations*, edited by P.E.A. Turchi and A. Gonis (Plenum New York, 1994), p. 361; S.-H. Wei, L.G. Ferreira, and A. Zunger, Phys. Rev. B **41**, 8240 (1990).
- ³⁷A. Sher, M. van Schilfgaarde, A.-B. Chen, and W. Chen, Phys. Rev. B **36**, 4279 (1987).
- ³⁸J.W.D. Connolly and A.R. Williams, Phys. Rev. B **27**, 5169 (1983).
- ³⁹A. Qteish, N. Motta, and A. Balzarotti, Phys. Rev. B **39**, 5987 (1989).
- ⁴⁰P. Hohenberg and W. Kohn, Phys. Rev. **136**, B864 (1964); W. Kohn and L.J. Sham, Phys. Rev. **140**, A1133 (1965).
- ⁴¹D. Vanderbilt, Phys. Rev. B **41**, 7892 (1990).
- ⁴²J. Furthmüller, P. Käckell, F. Bechstedt, and G. Kresse, Phys. Rev. B **61**, 4576 (2000).
- ⁴³U. Grossner, J. Furthmüller, and F. Bechstedt, Phys. Rev. B **58**, R1722 (1998); Appl. Phys. Lett. **74**, 3851 (1999).
- ⁴⁴J.P. Perdew and A. Zunger, Phys. Rev. B **23**, 5048 (1981).
- ⁴⁵H.J. Monkhorst and J.D. Pack, Phys. Rev. B **13**, 5188 (1976).
- ⁴⁶G. Kresse and J. Furthmüller, Comput. Mater. Sci. **6**, 15 (1996); Phys. Rev. B **54**, 11 169 (1996).
- ⁴⁷F. D. Murnaghan, Proc. Natl. Acad. Sci. USA **30**, 244 (1944).
- ⁴⁸A.F. Wright and J.S. Nelson, Phys. Rev. B **51**, 7866 (1995).
- ⁴⁹K. Kim, W.R.L. Lambrecht, and B. Segall, Phys. Rev. B **53**, 16 310 (1996).
- ⁵⁰K. Shimada, T. Sota, and K. Suzuki, J. Appl. Phys. **84**, 4951 (1998).
- ⁵¹D. Doppalapudi, S.N. Basu, K.F. Ludwig, Jr., and T.D. Moustakas, J. Appl. Phys. **84**, 1389 (1998).
- ⁵²E. Silveira, A. Tabata, J.R. Leite, R. Trentin, V. Lemos, T. Frey, D.J. As, D. Schikora, and K. Lischka, Appl. Phys. Lett. **75**, 3602 (1999).
- ⁵³A. Tabata, E. Silveira, J.R. Leite, R. Trentin, L.M.R. Scolfaro, V. Lemos, T. Frey, D.J. As, D. Schikora, and K. Lischka, Phys. Status Solidi B **216**, 769 (1999).
- ⁵⁴K.E. Miyano, J.C. Woicik, L.H. Robins, C.E. Bouldin, and D.K. Wickenden, Appl. Phys. Lett. **70**, 2108 (1997).